An Iterative Based Motion Correction for SPECT with Simulated Data

[1]Md. Nahid Hossain, [2]Kamila Afroj Quadir, [3]Adnan Kiber, [4]Roger Fulton

[1]National Institute of Nuclear Medicine & Allied Sciences (NINMAS), Dhaka
[2]Director (Retd) Bio-Science Division, Bangladesh Atomic Energy Commission
[3]Department of Electrical & Electronic Engineering, University of Dhaka
[4]Department of Medical Physics, Westmead Hospital, Australia

Correspondence Address: Md. Nahid Hossain, Professor & CSO, NINMAS, Block-D, BSMMU Campus, Shahbag, Dhaka. Email: nahidhssn@yahoo.com

ABSTRACT

Purpose: Single Photon Emission Computed Tomography (SPECT) is one of the important imaging modality in nuclear medicine used for diagnostic imaging of different organs of human body. Patient movement during the acquisition time is a well-known cause of artifacts in reconstructed SPECT data. These motion artifacts may significantly affect the diagnostic accuracy. Therefore, the motion correction of patients in tomography images is very much essential for more accurate diagnosis and hence achieves the quality of the images.

Objective: The aim of this project is to develop and evaluate a data driven approach to motion correction without necessity for motion tracking system.

Methods: It has been proposed a method to iteratively estimate and compensate this motion during the reconstruction. The rigid motion was estimated view-by-view in every iteration and then used to update the system matrix. The initial reconstructed image is motion contaminated; it can be used to generate a first rough motion estimate. This motion is taken into account in a reconstruction process to generate a motion-corrected image at the first iteration. Then the motion-corrected image and the motion estimate are alternately updated to increase the likelihood, the iterations are stopped when the updated motion seems to have converged. The image update is done by applying multiple iterations of the OSEM algorithm. A final iterative reconstruction was performed with the last motion estimate.

Results: The method was evaluated on simulations phantom study. From the simulations phantom data, we produced the several simulated motion induced data. Motion correction algorithms were applied with the simulated motion induced data. The quality of the reconstructed images was improved substantially after the compensation. Mean structural similarity was increased. In the simulation studies, most of the motion blurring in the reconstructed images disappeared after the compensation.

Conclusions: The proposed method effectively eliminated motion-induced artifacts in SPECT scans. Since only measured raw data are needed for the motion estimation and compensation, the proposed method can be applied retrospectively to SPECT scans affected by motion.

Keywords: SPECT, Iterative Reconstruction, Simulation, OSEM Algorithm, System Matrix, Motion Correction.

Bangladesh J. Nucl. Med. Vol. 26 No. 1 January 2023

Doi: https://doi.org/10.3329/bjnm.v26i1.64659

INTRODUCTION

Single Photon Emission Computed Tomography (SPECT) is one of the most essential imaging modalities used in nuclear medicine to diagnose and evaluate the physiological function of various human organs. A short-lived radiopharmaceutical is injected into the patient's body, and a series of two-dimensional (2D) images of radionuclide distribution are collected using the rotating gamma camera. These data are then reconstructed for the three-dimensional (3D) distribution of radioactivity to give a stack of transverse slices of the organ or region of interest. It is widely known that patient movement during the acquisition period causes artifacts in the reconstructed SPECT data. The data acquisition time is normally between five and thirty minutes, which is relatively high. The patient's movements cause the projection frames to be out of alignment, degrading the reconstructed image and perhaps introducing artifacts (1–5). These motion artifacts may severely impact diagnostic accuracy. Getting consistent projection data from the acquisition requires motion correction. When motion occurs between acquired projection views, consistency is lost and artifacts are generated in the reconstructed slices. Thus, it is quite necessary to compensate for the patient's motion in tomography images to produce quality images for a more accurate diagnosis. Motion correction requires knowledge of the six degrees of freedom (dof) of motion during the SPECT scan (6–8). An iterative-based motion correction scheme for SPECT has been proposed here. The rigid motion was estimated view-by-view in every iteration and then used to update the system matrix in SPECT data. We

have applied this method and tested simulated SPECT data with this algorithm.

OBJECTIVE

The objectives of this work were to develop and evaluate a data-driven approach to motion estimation that would allow motion correction to be applied without the necessity of a motion tracking system. Different sets of experiments are carried out on different kinds of simulated SPECT data to validate the motion correction procedure.

METHODS

Ordered subset expectation maximization (OSEM) reconstruction

In the presence of motion, the SPECT orbit is distorted into an effective orbit with an arbitrary shape. As this is problematic for analytical reconstruction, an iterative reconstruction algorithm is required. We used OSEM as the reconstruction algorithm.

$$\mu_q^{n+1} = \frac{\mu_q^n}{\sum_{p\in S_b} a_{pq}} \sum_{p\in S_b} a_{pq} \frac{g_p}{\sum_r a_{pr}\mu_r^n} \quad \ldots\ldots (1)$$

Where g is the log converted sinogram and Sb is one subset (consisting of b views) (9-11).

Motion estimation and compensation outline

The first task is to estimate the motion of the object for each of the acquired SPECT projections. This is attained by a 3D registration of the object to each of the 2D views independently. The first estimate of the 3D object is found with an initial reconstruction without motion compensation. Thus, this first image suffers from motion artifacts, which will significantly affect the pose estimation associated with each view. Though the 2D–3D registration process described below still captures part of the real motion, reconstruction with motion compensation based on these motion estimates improves the reconstruction. The more accurate motion estimates are produced by reiterating the process with this improved reconstruction.

Though the initial reconstructed image is motion-affected, it is used to produce a first rough motion estimate. This initial motion is taken into account in the reconstruction process, and a motion-corrected image is produced at the first iteration. Within this process, the motion-corrected image and the motion estimate are alternately updated, and the iterations are stopped when the updated motion seems to have converged. By applying multiple iterations of the OSEM algorithm, the image update is done.

Motion update

The estimated motion is acquired in the coordinate system of the detector. Because motion-corrected reconstruction requires motion in the world coordinate system, it is transformed to motion in the world coordinate system.

$$\left\{Q_\theta^{n,inc} \rightarrow T_\theta^{n,inc}\right\}_{\theta=0,\ldots\ldots,M} \ldots\ldots(2)$$

Where T is the 4×4 homogeneous matrix representation of the estimated motion in the world coordinate system, M is the total number of projection views. The transformation matrix obtained in the nth iteration was then used to update the previous motion estimate for every view, which was used in the next iteration (n+1),

$$\left\{T_\theta^{n+1} + T_\theta^n T_\theta^{n,inc}\right\}_{\theta=0,\ldots,M} \ldots\ldots\ldots (3)$$

Image update

The image representing the attenuation coefficients can be updated with iterative reconstruction after obtaining the motion. OSEM was used as the reconstruction algorithm. Instead of moving the reconstructed image in every view, rigid motion compensation is done by considering a coordinate system fixed to the object and incorporating the motion (now associated with the source-detector pair) into the system matrix.

$$\hat{T}_p^{n+1} = invert\left(T_p^{n+1}\right),$$

$$\mu_q^{n+1} = \frac{\mu_q^n}{\sum_{p\in S_b} \hat{T}_p^{n+1}(a_{pq})} \sum_{i\in S_b} \hat{T}_p^{n+1}\left(a_{pq}\right) \frac{f_i}{\sum_r \hat{T}_i^{n+1}(a_{pr})\mu_r^n} \quad \ldots\ldots\ldots (4)$$

Where ˆTp is a 4 × 4 transformation matrix applied to the projection line i. If Tp is the identity matrix for all projection lines, then Eq. (4) is the same as standard OSEM [Eq. (1)]. In SPECT, Tp is constant for all projection lines in one projection view; hence, the inversion is done for every single view. A distance-driven projection is used for interpolation during the (back) projection. The new estimate of the attenuation image is

then used for the next motion update (step 1). When the motion estimate has converged, a final reconstructed image with diagnostic quality must be produced for data.

Software validation for digital phantom experiment

Projection data for the simulations was obtained from a 64 x 64 x 64 voxel version of the digital Hoffman brain phantom. The voxels were 4.69 mm in each dimension. This phantom was projected using analytical projection software. A high-resolution parallel hole collimation with depth-dependent blur was modeled and included uniform tissue attenuation. To generate the attenuation map, the slices of the phantom were converted to binary, filled to provide uniform closed regions, Gaussian filtered to enlarge the extent of the brain, and finally converted back to binary gray levels. Thus, the attenuation slices followed the contour of the corresponding brain slices but were slightly larger to account for skull attenuation. The modeled attenuation coefficient was $\mu = 0.12\ cm^{-1}$. The projector generated 32 emission projections with dimensions of 32 x 32 pixels. Pixels were square, with a length of 9.38 mm. To model poisson noise in the projection data, each pixel was replaced by a random poisson deviate using the actual gray value as the distribution mean. The poisson-distributed values were generated after scaling the data so that the maximum total counts per projection were 50K. This value was intended to give a level of noise equivalent to a typical brain scan. We also converted the data into 128 x 128 x 128 voxels using the IDL program, and the voxels were 2.345 mm in each dimension.

Various rigid body transformations were applied to the digital Hoffman brain phantom to simulate projection sets corrupted by patient motion. After each transformation, it was projected and produced a different data set. Projections from the resulting sets were then combined to simulate a motion-corrupted acquisition. Projections were transferred as pairs since modelling was done with dual-180^o detector geometry. Motion was simulated to be discrete and to have occurred between projections. Motion occurring during the acquisition of a projection pair was not simulated.

Datasets

Six studies containing single movements were simulated. The six simulated sets were made to have considerable variation in the angular location and extent of movement and the magnitude of motion in each degree of freedom (DOF). Tx, Ty, Tz, Ry, Rx, and Rz are represented by the six DOF.

Movements were applied to the data and produced the data set D2, which is shown in Table 1, and the details of the simulated data are shown in Table 2.

Table 1: Details of data set D2 (Applied movements in the data D1)

Data (D2)	X in mm	Y in mm	Z in mm	X^0	Y^0	Z^0
D2-1	20	0	0	0	0	0
D2-2	0	20	0	0	0	0
D2-3	0	0	20	0	0	0
D2-4	0	0	0	10	0	0
D2-5	0	0	0	0	10	0
D2-6	0	0	0	0	0	10

Table 2: Details of Simulated Data set (Simulation from D1 and D2)

Without any Translation or Rotation Data-1 (D1)	Applied Translation in mm/Rotation in degrees Data-2 (D2)	Simulated data set	Simulated Data (SD)
Data D1	(20,0,0,0,0,0,)	Projection 1-30 from D1 Projection 31-60 from D2 Projection 61-90 from D1 Projection 91-120 from D2	Simulated Data SD1
	(0,20,0,0,0,0)		Simulated Data SD2
	(0,0,20,0,0,0)		Simulated Data SD3
	(0,0,0,10,0,0)		Simulated Data SD4
	(0,0,0,0,10,0)		Simulated Data SD5
	(0,0,0,0,0,10)		Simulated Data SD6

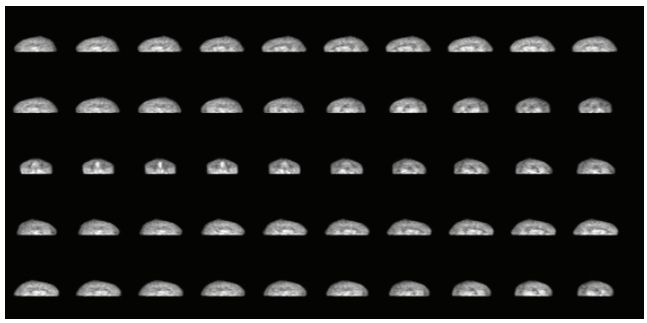

Figure 1: Projection view of the simulated brain phantom data

RESULTS

The effects of motion compensation were evaluated by visual assessment and quantitative analysis in the simulation studies.

The reconstructed motion-corrected images and the uncorrected images were compared in all views with similarity metrics. The reconstructed images of the same slices of the simulated data with and without motion corrections are shown in the figures. The three parts of the slice were named transaxial, sagittal, and coronal.

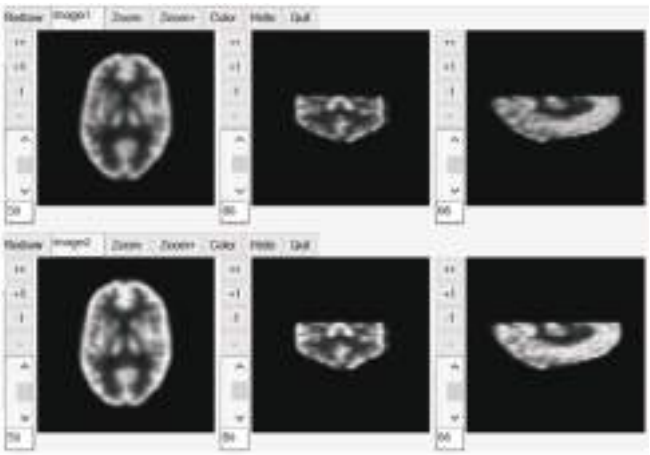

Figure 2: Reconstructed images with and without motion correction for motion free data

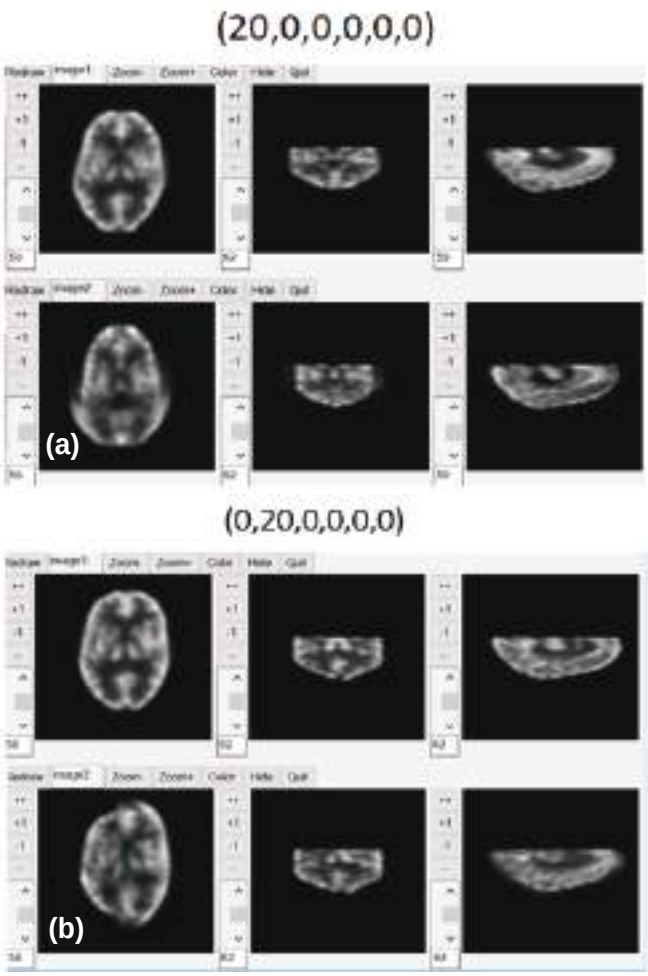

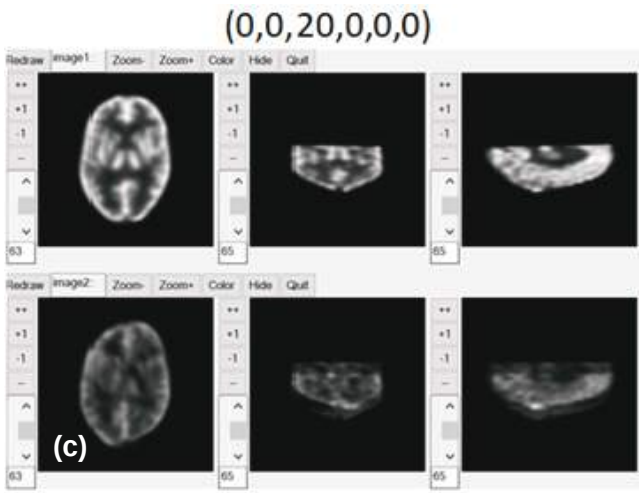

Figure 3: Reconstructed images with and without motion correction for translational motion induced data (The top image shows motion-corrected slices, while the bottom image shows motion-uncorrected slices) (a) Simulated Data SD1, (b) Simulated Data SD2 and (c) Simulated Data SD3

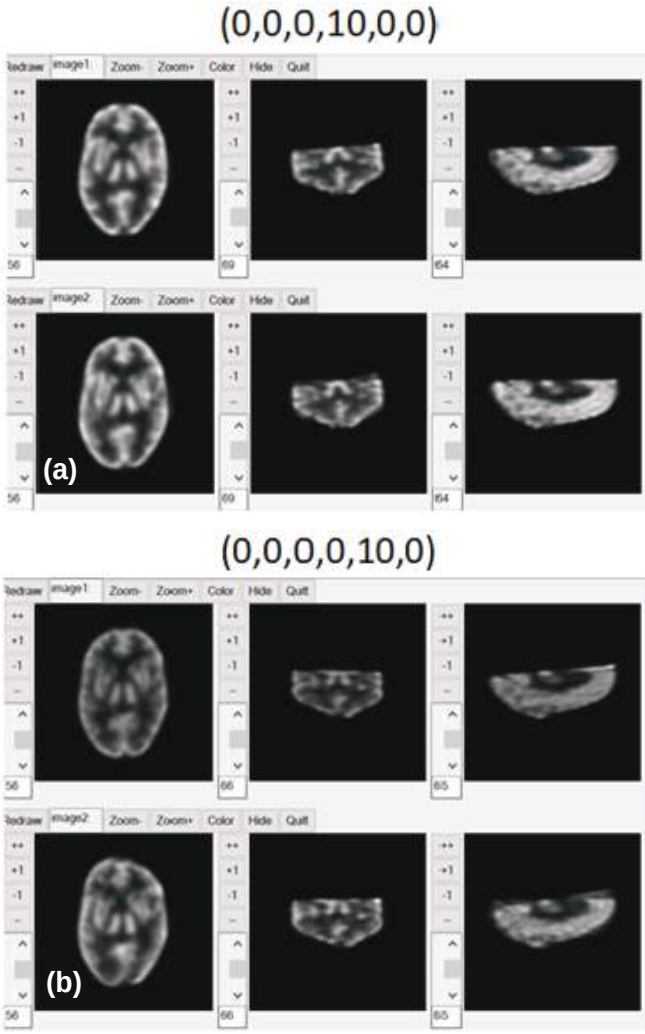

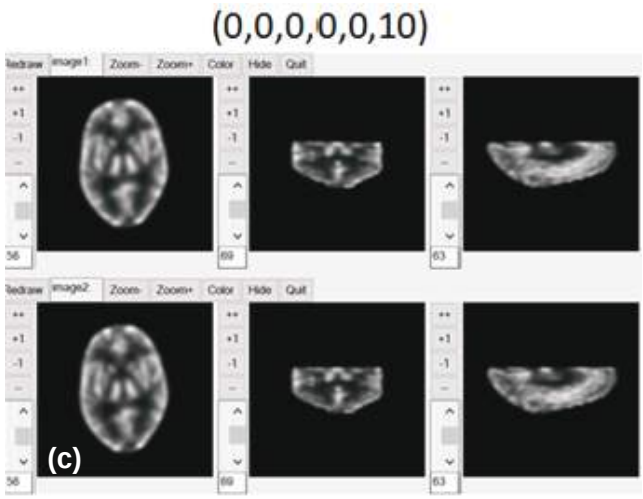

Figure 4: Reconstructed images with and without motion correction for rotational motion induced data (The top image shows motion-corrected slices, while the bottom image shows motion-uncorrected slices) (a) Simulated Data SD4, (b) Simulated Data SD5 and (c) Simulated Data SD6.

The effects of motion compensation were evaluated by visual assessment and quantitative analysis in the simulation studies. The reconstructed motion-corrected images and the uncorrected images were compared in all views with similarity metrics. The reconstructed images of the same slices of simulated data with and without motion correction are shown in the figures. The three parts of the slice were named transaxial, sagittal, and coronal.

At first, we applied our motion correction algorithm to the original simulated data, which was motion free. In Figure 2, we have seen the slices of these reconstructed data, and it is clearly visible that both slices were the same.

A 20-mm shift was applied in the X direction in the selected projection frames of SD1 data. The reconstructed slices were shown in Figure 3(a). It was demonstrated that some distortion or motion artifact was produced in the transaxial slice in the uncorrected slices, which was clearly removed in the corrected slices. We also compared these corrected slices to the ones in Figure 2, which were nearly identical and appeared to be motion-free slices with no artifacts.

In Data SD2, a 20 mm shift was applied in the Y direction in the selected projection frames. The reconstructed slices are shown in Figure 3(b). Uncorrected slices revealed some distortion or artifact in the upper and lower parts of the transaxial slice in the Y direction, as well as some distortion in the sagittal view. These distortions were clearly removed in the corrected slices.

As with SD1 and SD2, a 20-mm shift was applied in the Z direction in the selected projection frames in SD3. The reconstructed slices were shown in Figure 3(c). The motion has significantly affected all uncorrected reconstructed slices in transaxial, coronal, and sagittal views. These distortions were clearly removed in the corrected slices. It looks like almost motionless slices without any distortion.

In SD4, SD5, and SD6, 10^{O} shifts were applied in the X, Y, and Z directions, which were called yaw, pitch, and roll, respectively. Figures 4(a), 4(b), and 4(c) show the all-reconstructed slices for these three data points. The motion has slightly affected all uncorrected reconstructed slices in transaxial, coronal, and sagittal views. These were clearly removed in the corrected slices.

The corrected and uncorrected reconstructed images of a selected simulation using the software are shown in the figures. Most of the distortions were eliminated. The true image was much more similar to the corrected image than the uncorrected one. Figures show the overall improvement across all image slices in all studies with different motions.

DISCUSSIONS

The data-driven approach was validated in computer simulations. Different rigid-body transformations were applied to simulate projection sets corrupted by motion on the digital Hoffman brain phantom. Each transformation was projected as described above. The projections from the resulting sets were then combined to simulate a motion-corrupted acquisition. Since we were simulating the geometry of a dual-180^{O} detector, projections were always transferred as orthogonal pairs. The simulated motion was discrete and appeared to have happened in between projections. Motion occurring during the acquisition of a projection pair was not simulated. Datasets containing single and multiple six-DOF motions were simulated. Motions varied in magnitude, angular location, and angular extent. Corrected slices displayed a clear reduction in symmetry and perfusion defects. Most of the distortions were eliminated in all corrected and reconstructed images.

The true image was much more similar to the corrected image than the uncorrected one. Figures show the overall improvement across all image slices in all studies with different motions. There was no requirement that attenuation be incorporated in the estimation process, enabling considerable benefits in performance.

CONCLUSION

We proposed a general rigid-body motion correction approach for SPECT scans. It was a novel data-driven approach for correcting motion for SPECT using only acquired raw data. Our method is totally free of external devices and has the potential to be fully automated. There is no prerequisite knowledge of motion. It is easily adaptable to various types of collimation and multi-detector geometries.

Acknowledgement

This work was carried out within the framework of the International Atomic Energy Agency's (IAEA) Doctoral Coordinated Research Project (CRP) E.2.40.19 on "Advances in Medical Imaging Techniques." The authors would like to acknowledge the IAEA for providing support for this program.

REFERENCES

1. J.A. Cooper, P.H. Neumann, and B.K. McCandless. Effect of patient motion on tomographic myocardial perfusion imaging. J. Nucl. Med., 33(8):1566-1571, 1992.
2. J. Friedman, K. Van Train, J. Maddahi, A. Rozanski, F. Pringent, J. Bitendorf, A. Waxman, and D.S. Berman. Upward creep of the heart: a frequent source of reversible defects during thallium-201 stress-redistribution SPECT. J. Nucl. Med., 30(10):1718-1722, 1989.
3. Eisner RL, Churchwell A, Noever T, et al., Quantitative analysis of the tomographic thallium-201 myocardial bullseye display: critical role of correcting patient motion. J. Nucl. Med., 29:91-97, 1988.
4. Tsui BMW, Segars WP, and Lalush DS. Effects of upward creep and respiratory motion in myocardial SPECT. IEEE Trans. Nucl. Sci., 47:1192-1195, 2000.
5. Botvinick EH, Zhu YY, O'Connell WJ, and Dae MW. A quantitative assessment of patient motion and its effect on myocardial perfusion SPECT images. J. Nucl. Med., 34:303-310, 1993.
6. Saeed Sarkar, Mohammad A. Oghabian, Iraj Mohammadi, Alireza Mohammadpour and Arman Rahmim. A Linogram/Sinogram Cross-Correlation Method for Motion Correction in Planar and SPECT Imaging. IEEE Transactions on Nuclear Science, Vol. 54, no. 1, February 2007.
7. Q. S. Chen, M. Defrise, F. Deconinck, P. R. Franken, and M. H. Jonckheer, "Detection and correction of patient movements in SPECT imaging," J. Nucl. Med. Technol., vol. 21, no. 4, pp. 198–205, 1993.
8. J. M. Wheat and G. M. Currie, "Incidence and characterization of patient motion in myocardial perfusion SPECT: part 1," J. Nucl. Med. Technol., vol. 32, pp. 60–65, 2004.
9. Kim, J., J. Nuyts, A. Kyme, Z. Kuncic, and R. Fulton (2015b). A rigid motion correction method for helical computed tomography (CT)." In: Phys. Med. Biol. 60.5, pp. 2047-73. doi: 10.1088/0031-9155/60/5/2047.
10. Hudson, H. M. and R. S. Larkin (1994). \Ordered subsets of projection data." In: IEEE Trans. Med. Imaging 13.4, pp. 601-609.
11. Nuyts, J., B. D. Man, P. Dupont, M. Defrise, P. Suetens, and L. Mortelmans (1998). \Iterative reconstruction for helical CT: a simulation study." In: Phys. Med. Biol. 43.4, pp. 729-737. doi: 10.1088/0031-9155/43/4/003.